Controlled Synthesis of Mg-MOF-74 and Its CO_2 Adsorption in Flue Gas

Chunling Xin *, Shufen Hou , Lei Yu , Xiaojing Zhou , Fan Yang , Xia Wang , Lili Liu

Posted Date: 26 January 2024

doi: 10.20944/preprints202401.1902.v1

Keywords: Metal-organic frameworks; Mg-MOF-74; CO2 adsorption; Flue gas; Regeneration performance

Article

Controlled Synthesis of Mg-MOF-74 and Its CO_2 Adsorption in Flue Gas

Chunling Xin, Shufen Hou, Lei Yu, Xiaojing Zhou, Fan Yang, Xia Wang * and Lili Liu *

Department of Chemistry and Chemical & Environmental Engineering,Weifang University, Weifang 261061, Shandong, China

* correspondence: 20160012@wfu.edu.cn (X.W.); liulili122@wfu.edu.cn (L.L.)

Abstract: Yellow nanorod Mg-MOF-74 was obtained by solvothermal synthesis method. XRD、N_2 adsorption-desorption isotherms、SEM and TGA results suggest that the particle size of Mg-MOF-74 reaches 400 nm after the introduction of sodium acetate in the precursor of Mg-MOF-74. Besides, the morphology of Mg-MOF-74 was changed from cauliflower to rod particles. At the same time, the BET specific surface area and pore volume of Mg-MOF-74 were also increased a lot. Then the CO_2 dynamic adsorption capacity of Mg-MOF-74 was measured by self-made fix bed under 30 ℃、0.1 bar CO_2 partial pressure. The results show that the CO_2 adsorption capacity of Mg-MOF-74-N2 reaches 3.67 mmol/g and its CO_2 adsorption capacity remains unchanged after 10 times CO_2 adsorption-desorption cycles.

Keywords: Metal-organic frameworks; Mg-MOF-74; CO_2 adsorption; Flue gas; Regeneration performance

1. Introduction

Excessive CO_2 emissions caused by the burning of fossil fuels and human activities have led to increasing global warming, melting glaciers, frequent disaster weather, and sharp decline in plant and animal diversity. The United Nations (IPCC) has issued a goal of reducing global CO_2 emissions by 41% to 72% by 2050 compared with 2010[1]. In China, power plants are the concentrated source of CO_2 emissions, accounting for 40% of the total CO_2 emissions. Controlling CO_2 emissions in the flue gas of power plants is the key to achieve CO_2 emission reduction goals. At present, CO_2 capture and storage (CCS) technology is the key technology to mitigate and control CO_2 emissions, and reducing the cost of capture stage is the top priority in implementing this technology. Based on the low CO_2 content in the flue gas of power plant, the commonly used CO_2 capture methods include absorption, adsorption, membrane separation and low temperature distillation. Among them, adsorption method has the advantages of simple process, mild operating conditions, low energy consumption and no corrosion to equipment, so it is the most promising capture method at present. At present, many materials used in the field of CO_2 adsorption are activated carbon, molecular sieve, metal oxides, metal-organic skeleton materials (MOFs) [2–5]. High CO_2 adsorption capacity, fast absorption/desorption rate, good selectivity, good adsorption stability and low regenerative energy consumption are the conditions for the preparation of excellent CO_2 adsorbents. MOFs is a new type of crystalline porous material composed of metal ions and organic ligands[6]. Its high specific surface area developed void structure and adjustable chemical composition make this material widely used in gas adsorption and separation[7–11], drug carrier[12], catalysis[13], sensor[7,14] and other fields. With the development of nanotechnology, nanoscale MOFs have attracted the attention of scientists because of their special morphology, particle size and other excellent characteristics. At present, the synthesis methods of nanometer MOFs include direct precipitation method, microwave assisted method, hydrothermal/solvothermal synthesis method, mechanical method and so on.

For example, the Ahn[15] research group reported a method for the preparation of nano-scale Mg-MOF-74 by ultrasonic chemistry, which uses triethylamine as the deprotonation agent and

greatly reduces the reaction time. The Sun[16] research group used polyethylpyrrolidone and ammonia water to regulate the morphology and particle size of Mg-MOF-74. In addition, N_2 adsorption and desorption results also show that the morphology and particle size of Mg-MOF-74 affect the adsorption properties of the gas. Chen[12] research group prepared Mg-MOF-74 with particle size less than 200 nm by two-step method and explored its application in drug carrier. Zhang[17] et al. reported that a Mg-MOF-74/sodium alginate composite aerogel were prepared by loading Mg-MOF-74 on sodium alginate sheets followed by directional freeze-drying. The experimental data showed that the composite achieved CO_2 adsorption of 2.461 mmol/g at 298 K. This may be due to the hierarchical pore structure formed by the composite aerogel. The micropores/mesopores structure of Mg-MOF-74 can improve the interaction between CO_2 and the adsorbent and enhance the gas mass transfer rate[1,18,19]. However, Up to now, in the reported MOFs, there are still few studies on CO_2 adsorption in flue gas for nanoscale Mg-MOF-74.

In this paper, nanorod Mg-MOF-74 particles were synthesized by a simple solvothermal method without surfactants. The morphology and particle size of MOFs were adjusted by controlling the concentration of sodium acetate (NaAc). The dynamic adsorption performance of nano-scale Mg-MOF-74 under simulated flue gas environment was tested by a self-made fixed bed, which provided a theoretical basis for the design and synthesis of CO_2 adsorbent suitable for power plant flue gas environment.

2. Experimental part

2.1. Reagents and characterization

2,5-dihydroxyterephthalic acid (H_4DOBDC), magnesium nitrate hexahydrate ($Mg(NO_3)_2 \bullet 6H_2O$), N,N-dimethylformamide (DMF), anhydrous methanol (CH_3OH), sodium acetate (NaAc) were used in Shanghai Aladdin Reagent Co., LTD. The reagents used were all analytically pure. CO_2 (high purity, Beijing Beiwen Gas Factory), N_2 (high purity, TISCO Gas Factory)

X-ray diffraction analysis was performed by D8 Advance X-ray diffractometer of Nikaku, using Cu Kα radiation (λ=0.154 nm), metal Ni filter, tube pressure 40 kV, tube flow 30 mA. The N_2 adsorption and desorption isotherm of the sample at 77 K was determined by ASAP 2020 automatic physical adsorption instrument. The sample was vacuumed and degassed at 200 ℃ for one night before the test. The microstructure and morphology of the sample were observed on JSM-7001 thermal field emission scanning electron microscope. The sample was coated with conductive adhesive and scanned after gold spraying. During the test, the acceleration voltage is 5-10 kV. Rigaku TG thermogravimetric analyzer was used to study the thermal stability of the sample. Under N_2 inert atmosphere, the weight of the sample was 10 mg. The thermogravimetric curve of the sample was tested in the range of 25-600 ℃, and the heating rate was 10 ℃/min.

2.2. Synthesis of Mg-MOF-74

0.674 g H_4DOBDC and 2.8 g $Mg(NO_3)_2 \bullet 6H_2O$ were added to 300 mL DMF/EtOH/H_2O mixed solution with a volume ratio of 15:1:1, and stirred until dissolved. 0-4 equal amounts of NaAc were added to the mixture, then the reaction liquid was placed in a crystallization kettle and reacted in an oven at 125 ºC for 20 h. Finally, the mother liquid was poured out to obtain yellow microcrystals. The obtained crystals were impregnated into methanol solution for replacement, once every two days for three consecutive times, and the crystals were placed in a 200 ºC vacuum drying oven to remove the solvent and obtain Mg-MOF-74. The resulting sample is named Mg-MOF-74-N(0-4), where N represents NaAc and 0-4 represents the equivalent amount added to NaAc.

2.3. Evaluation of adsorbents

The CO_2 dynamic adsorption breakthrough experiment of the adsorbents was measured on a self-built fixed bed. Appropriate amount of adsorbent was pressed through the screen, and 20-40 mg of adsorbent was put into a U-shaped quartz tube with an inner diameter of 5 mm. The adsorbent was activated in Ar atmosphere at 200℃ for 6 h with a gas volume flow rate of 60 mL/min and a

 doi:10.20944/preprints202401.1902.v1

constant inlet concentration. After the activation, drop to the required temperature, switch the gas valve to the mixture of CO_2 and N_2 (CO_2/N_2=1:9), adjust the mass flowmeter to the required gas flow, use gas chromatography to detect the concentration of the air outlet, record the concentration of the air outlet every 10 s, until the CO_2 concentration of the air outlet is close to or even the same as the concentration of the air inlet, then stop the detection. Then, in argon atmosphere, desorption at high temperature. After desorption, the temperature was lowered to the specified adsorption temperature and then the CO_2 adsorption experiment was carried out.

According to the concentration of CO_2 at the air outlet, the CO_2 penetration curve of the material can be obtained, and the CO_2 adsorption capacity can be calculated according to the penetration curve. The specific calculation formula is as follows:

$$q = \frac{Q(t_s - t_0)C_{in}}{22.4W} \tag{1}$$

$$t_s = \int_0^t \left(1 - \frac{C_{out}}{C_{in}}\right) d_t \tag{2}$$

where, t_s(s) is the average residence and adsorption time, t_0(s) is the average residence and adsorption time of the empty bed, C_{in} and C_{out} are the CO_2 concentration of the import and export respectively, that is, the volume fraction of CO_2 in the gas, q is the CO_2 equilibrium adsorption capacity of the material (mmol/g), and Q is the volume flow rate of the mixture (mL/s). W is the mass of the adsorbent.

2. Results and discussion

To investigate the effect of NaAc concentration on the structure of Mg-MOF-74, 0-2 equal amounts of NaAc were added to the precursor solution of Mg-MOF-74, and the resulting products were named MG-MOF-74-N0, MG-MOF-74-N0.5, MG-MOF-74-N1, MG-MOF-74-N2, respectively. The obtained samples were characterized by XRD, and the results were shown in Figure 1. It can be seen from Figure 1 that the XRD diffraction peak of the sample is consistent with the XRD pattern reported in the literature[20]. After adding NaAc, the diffraction peak of Mg-MOF-74 did not change, indicating that the introduction of NaAc did not destroy the crystal structure. However, after adding NaAc, the diffraction peak intensity decreases rapidly, and with the increase of NaAc concentration, the diffraction peak intensity decreases gradually. The results showed that the crystallinity of the crystals decreased after the introduction of NaAc into the precursor solution of Mg-MOF-74.

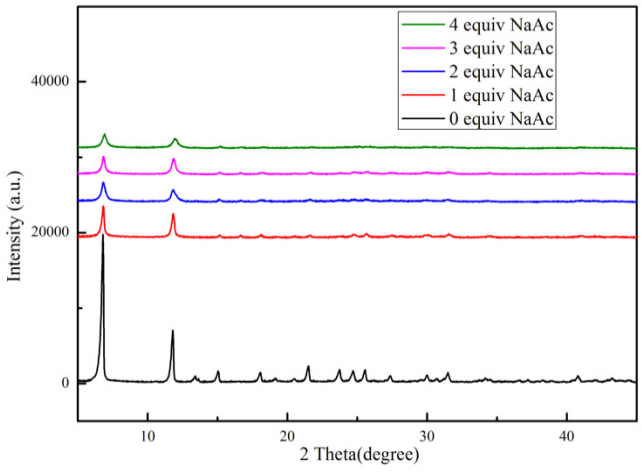

Figure 1. XRD pattern of Mg-MOF-74 synthesized by adding different concentrations of NaAc.

 doi:10.20944/preprints202401.1902.v1

To further investigate the effect of NaAc concentration on the crystal morphology of Mg-MOF-74, the samples were characterized by SEM. As can be seen from the Figure 2, without adding NaAc, the obtained Mg-MOF-74 showed the morphology of cauliflower, consisting of rod-like particles aggregated into cauliflower shape, which was consistent with the literature reports. Its particle size is about 17 μm, and after adding 0.5 equivalent amount of NaAc, the size of cauliflower particles is about 13 μm. When the concentration of NaAc increased to 1 equal amount, the rod-like particles gathered into cauliflower dispersed, Mg-MOF-74-N1 mainly presented rod-like particles, the length of rod-like particles was about 5μm, and the diameter of rod-like particles was about 1 micron. When the concentration of NaAc was further increased to 2 equal amounts, the obtained Mg-MOF-74-N2 was still rod-like particles with a diameter of about 3μm and uniform distribution, and the diameter of the particles was about 400 nm. With the increase of NaAc concentration, the particle size of Mg-MOF-74 decreased from micron to nanometer.

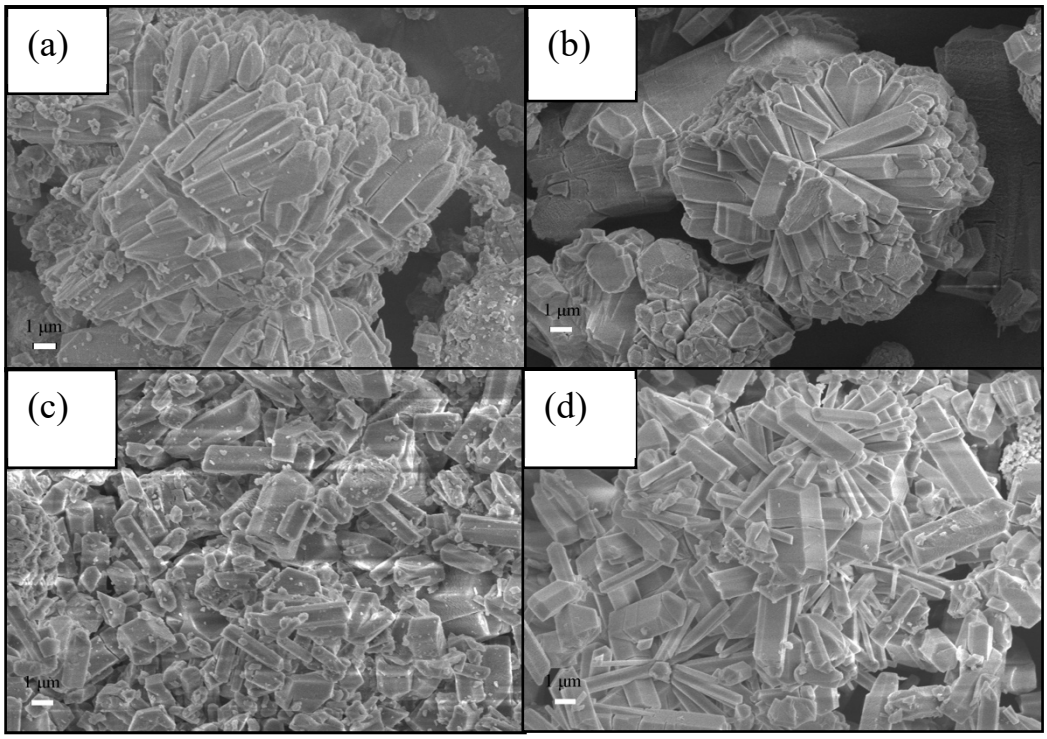

Figure 2. SEM images of Mg-MOF-74-N0(a), Mg-MOF-74-N0.5(b), Mg-MOF-74-N1(c), Mg-MOF-74-N2(d).

To further test the pore structure properties of nanoscale Mg-MOF-74, N2 adsorption and desorption experiments were performed on the sample, and the results were shown in Figure 3. It can be seen from the N2 adsorption and desorption isotherm of the sample that the adsorption isotherm of Mg-MOF-74 synthesized without adding NaAc conforms to the Class I adsorption curve, indicating that the pores in Mg-MOF-74 are micropores. The H3 hysteresis ring in the adsorption isotherm of Mg-MOF-74-N2 indicates the presence of mesoporous pores in the sample. This may be due to a reduction in the size of the crystals, resulting in the accumulation of holes. The pore volume, specific surface area and pore diameter of Mg-MOF-74 and MG-MOF-74-N2 are listed in Table 1. It can be seen from the data in the table that the pore volume increases with the increase of the specific surface area of MG-MOF-74-N2, and the pore size remains almost unchanged. This shows that the addition of NaAc helps to increase the specific surface area of the crystal, and the increase of pore volume is due to the formation of many accumulation holes due to the reduction of crystal size, which leads to the increase of the total pore volume of the sample[21].

 doi:10.20944/preprints202401.1902.v1

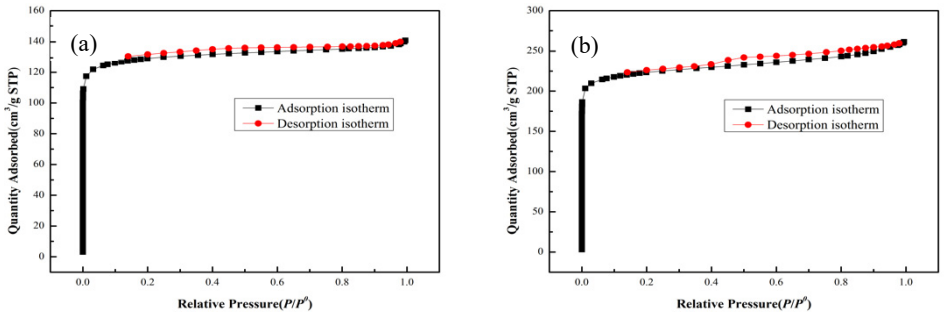

Figure 3. N_2 adsorption and desorption isotherms of Mg-MOF-74-N0(a) and Mg-MOF-74-N2(b).

Table 1. Pore volume, specific surface area and pore size of Mg-MOF-74 and MG-MOF-74-N2.

Samples	Specific area(m^2/g)	Pore volume (cm^3/g)	Pore size (nm)
Mg-MOF-74	570.3	0.218	0.91
Mg-MOF-74-N2	624.7	0.264	0.92

To further test the thermal stability of Mg-MOF-74 crystal, we performed thermogravimetric analysis of the sample, and the results were shown in Figure 4. The weight loss from room temperature to 100 °C is attributed to the moisture adsorbed in the Mg-MOF-74 hole, and the weight loss from 100 to 250 °C is attributed to the solvent adsorbed in the hole[22]. It can be seen from the thermogravimetric curve that the weight of MG-MOF-74-N2 no longer decreases at 500 °C, while Mg-MOF-74 continues to lose weight at 600 °C, so the thermal stability of MG-MOF-74-N2 is significantly improved compared with Mg-MOF-74.

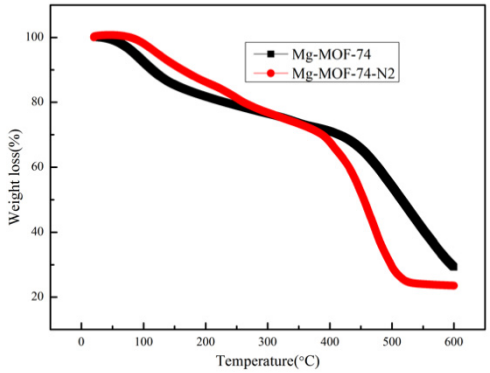

Figure 4. Thermogravimetric analysis of Mg-MOF-74 and Mg-MOF-74-N2.

A self-made fixed bed was used to test the dynamic CO_2 adsorption performance of nano-scale Mg-MOF-74 in simulated flue gas environment, and the dynamic adsorption penetration curve was shown in Figure 5. According to formula (1) and (2), the dynamic CO_2 adsorption capacity of Mg-MOF-74-N2 under 30 °C and 0.1 bar CO_2 partial pressure is 3.63 mmol/g, which is much higher than the 1.62 mmol/g of Mg-MOF-74-N0 under the same conditions. This may be due to the increase of the specific surface area and pore volume of the synthesized Mg-MOF-74-N2 nanoparticles after the addition of NaAc, so its CO_2 adsorption performance is also improved.

 doi:10.20944/preprints202401.1902.v1

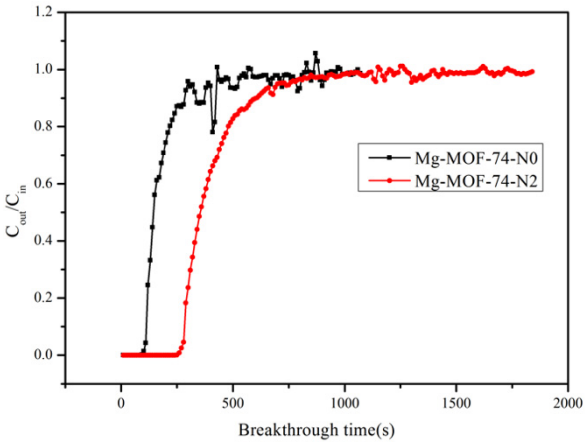

Figure 5. CO_2 dynamic adsorption penetration curves of Mg-MOF-74-N0 and Mg-MOF-74-N2 at 30 ℃ and 0.1 bar CO_2 partial pressure.

To test the regeneration performance of Mg-MOF-74-N2, we used a fixed bed to test the CO_2 cycling absorption and desorption experiment of the adsorbent at 30 ℃ and 0.1 bar CO_2 partial pressure, and the results were shown in Figure 6. When the CO_2 adsorption is saturated, the temperature rises to 200 ℃ for desorption under Ar gas atmosphere, and then the temperature drops to 30 ℃ for CO_2 adsorption under 0.1bar CO_2 partial pressure. After 10 cycles of adsorption and desorption, the CO_2 adsorption capacity of the adsorbent under 30 ℃ and 0.1bar CO_2 partial pressure almost remains unchanged. The results indicated that the regeneration performance of Mg-MOF-74-N2 was high.

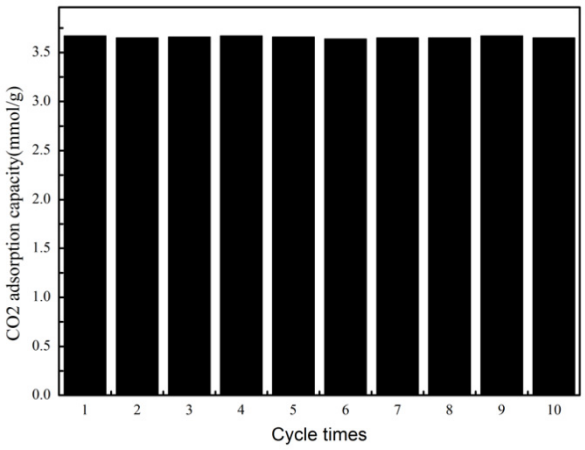

Figure 6. CO_2 adsorption capacity of Mg-MOF-74-N2 after 10 absorption and desorption cycles at 30 ℃ and 0.1 bar CO_2 partial pressure.

3. Conclusion

Mg-MOF-74 was synthesized by solvothermal synthesis method. After adding NaAc into the precursor solution, the crystal morphology changed from cauliflower type to rod-like particles, and the particle size changed from micron to nanometer particles. The dynamic CO_2 adsorption performance of Mg-MOF-74 under simulated flue gas environment was tested. The results showed that the CO_2 adsorption performance of nanoscale MG-MOF-74-N2 synthesized by adding NaAc was

significantly improved, and the CO_2 adsorption capacity reached 3.63 mmol/g at 30°C and 0.1 barCO_2 partial pressure.

Acknowledgments: This paper is supported by the National Natural Science Foundation of China (22108208).

Conflicts of interest: The authors declare no conflicts of interest.

References

1. Xin, C. L.; Ren, Y.; Zhang, Z. F.; Liu, L. L.; Wang, X.; Yang, J. M., Enhancement of Hydrothermal Stability and CO2 Adsorption of Mg-MOF-74/MCF Composites. *Acs Omega* **2021,** 6, (11), 7739-7745.
2. Choi, S.; Drese, J. H.; Jones, C. W., Adsorbent Materials for Carbon Dioxide Capture from Large Anthropogenic Point Sources. *Chemsuschem* **2009,** 2, (9), 796-854.
3. Li, W.; Bollini, P.; Didas, S. A.; Choi, S.; Drese, J. H.; Jones, C. W., Structural Changes of Silica Mesocellular Foam Supported Amine-Functionalized CO_2 Adsorbents Upon Exposure to Steam. *ACS Appl. Mat. Interfaces* **2010,** 2, (11), 3363-3372.
4. Comotti, A.; Fraccarollo, A.; Bracco, S.; Beretta, M.; Distefano, G.; Cossi, M.; Marchese, L.; Riccardi, C.; Sozzani, P., Porous dipeptide crystals as selective CO_2 adsorbents: experimental isotherms vs. grand canonical Monte Carlo simulations and MAS NMR spectroscopy. *Crystengcomm* **2013,** 15, (8), 1503-1507.
5. Halabi, M. H.; de Croon, M. H. J. M.; van der Schaaf, J.; Cobden, P. D.; Schouten, J. C., Kinetic and structural requirements for a CO_2 adsorbent in sorption enhanced catalytic reforming of methane - Part I: Reaction kinetics and sorbent capacity. *Fuel* **2012,** 99, 154-164.
6. Chui, S. S., A Chemically Functionalizable Nanoporous Material $[Cu_3(TMA)_2(H_2O)_3]n$. *Science* **1999,** 283, (5405), 1148-1150.
7. Thomas, S.; Mayr, F.; Gagliardi, A., Adsorption and sensing properties of SF_6 decomposed gases on Mg-MOF-74. *Solid State Communications* **2023,** 363, 115120-115124.
8. Yang, R. H.; Ullah, S.; Chen, X.; Ma, J. X.; Gao, Y.; Wang, Y. J.; Luo, G. S., Selective adsorption of liquid long-chain α-olefin/paraffin on Mg-MOF-74: Adsorption behavior and interaction mechanism. *Nano Research* **2023,** 16, (1), 1595-1605.
9. Mallick, A.; Mouchaham, G.; Bhatt, P. M.; Liang, W.; Belmabkhout, Y.; Adil, K.; Jamal, A.; Eddaoudi, M., Advances in Shaping of Metal–Organic Frameworks for CO_2 Capture: Understanding the Effect of Rubbery and Glassy Polymeric Binders. *Industrial & Engineering Chemistry Research* **2018,** 57, (49), 16897-16902.
10. Alezi, D.; Belmabkhout, Y.; Suyetin, M.; Bhatt, P. M.; Weselinski, L. J.; Solovyeva, V.; Adil, K.; Spanopoulos, I.; Trikalitis, P. N.; Emwas, A. H.; Eddaoudi, M., MOF Crystal Chemistry Paving the Way to Gas Storage Needs: Aluminum-Based soc-MOF for CH_4,O_2, and CO_2 Storage. *J Am Chem Soc* **2015,** 137, (41), 13308-13318.
11. CREAMER, A. E.; GAO, B., Carbon-Based Adsorbents for Postcombustion CO_2 Capture: A Critical Review. *Environmental Science & Technology* **2016,** 50, (14), 7276-7289.
12. Hu, J. Q.; Chen, Y.; Zhang, H.; Chen, Z. X., Controlled syntheses of Mg-MOF-74 nanorods for drug delivery. *Journal of Solid State Chemistry* **2021,** 294, 121853.
13. Chen, C.; Li, B. X.; Zhou, L. J.; Xia, Z. F.; Feng, N. J.; Ding, J.; Wang, L.; Wan, H.; Guan, G. F., Synthesis of Hierarchically Structured Hybrid Materials by Controlled Self-Assembly of Metal Organic Framework with Mesoporous Silica for CO_2 Adsorption. *Acs Applied Materials & Interfaces* **2017,** 9, (27), 23060-23071.
14. Yu, C. P.; Cui, J. W.; Wang, Y.; Zheng, H. M.; Zhang, J. F.; Shu, X.; Liu, J. Q.; Zhang, Y.; Wu, Y. C., Porous HKUST-1 derived CuO/Cu_2O shell wrapped $Cu(OH)_2$ derived CuO/Cu_2O core nanowire arrays for electrochemical nonenzymatic glucose sensors with ultrahigh sensitivity. *Applied Surface Science* **2018,** 439, 11-17.
15. Yang, D. A.; Cho, H. Y.; Kim, J.; Yang, S. T.; Ahn, W. S., CO_2 capture and conversion using Mg-MOF-74 prepared by a sonochemical method. *Energy & Environmental Science* **2012,** 5, (4), 6465.
16. Yao, Z. Y.; Guo, J. H.; Wang, P.; Liu, Y.; Guo, F.; Sun, W. Y., Controlled synthesis of micro/nanoscale Mg-MOF-74 materials and their adsorption property. *Mater. Lett.* **2018,** 223, 174-177.
17. Peng, X. Q.; Zhang, J.; Sun, J. Q.; Liu, X. C.; Zhao, X. F.; Yu, S. M.; Yuan, Z. P.; Liu, S. J.; Yi, X. B., Hierarchically Porous Mg-MOF-74/Sodium Alginate Composite Aerogel for CO_2 Capture. *Acs Applied Nano Materials* **2023,** 6, (18), 16694-16701.
18. Xin, C.; Zhan, H.; Huang, X.; Li, H.; Zhao, N.; Xiao, F.; Wei, W.; Sun, Y., Effect of various alkaline agents on the size and morphology of nano-sized HKUST-1 for CO_2 adsorption. *RSC Advances* **2015,** 5, (35), 27901-27911.
19. Xin, C.; Jiao, X.; Yin, Y.; Zhan, H.; Li, H.; Li, L.; Zhao, N.; Xiao, F.; Wei, W., Enhanced CO_2 Adsorption Capacity and Hydrothermal Stability of HKUST-1 via Introduction of Siliceous Mesocellular Foams (MCFs). *Industrial & Engineering Chemistry Research* **2016,** 55, (29), 7950-7957.
20. Chakraborty, A.; Maji, T. K., Mg-MOF-74@SBA-15 hybrids: Synthesis, characterization, and adsorption properties. *Apl Materials* **2014,** 2, (12), 124107-124113.

 doi:10.20944/preprints202401.1902.v1

21. Li, F. F.; Chen, Y. N.; Gong, M.; Chen, A. J.; Li, L.; Zhang, Z. T.; Liu, Y.; Dan, N. H.; Li, Z. J., Core-shell structure Mg-MOF-74@$MSiO_2$ with mesoporous silica shell having efficiently sustained release ability of magnesium ions potential for bone repair application. *Journal of Non-Crystalline Solids* **2023,** 600, 10.1016/j.jnoncrysol.2022.122018.
22. An, H. F.; Tian, W. J.; Lu, X.; Yuan, H. M.; Yang, L. Y.; Zhang, H.; Shen, H. M.; Bai, H., Boosting the CO_2 adsorption performance by defect-rich hierarchical porous Mg-MOF-74. *Chemical Engineering Journal* **2023,** 469, 10.1016/j.cej.2023.144052.